Hindawi
Geofluids
Volume 2021, Article ID 6669921, 11 pages
https://doi.org/10.1155/2021/6669921

Research Article

Experimental Study on Blockage Mechanism and Blockage Locations for Polymer-Flooded Reservoirs in the Henan Oilfield

Yu Li, Meilong Fu, Baofeng Hou, Zhiyuan Zhang, and Ruiyi Sun

School of Petroleum Engineering, Yangtze University, Wuhan 430100, China

Correspondence should be addressed to Meilong Fu; 805817751@qq.com

Received 23 November 2020; Revised 10 March 2021; Accepted 30 March 2021; Published 18 April 2021

Academic Editor: Shiyuan Zhan

To address the issues of reservoir blockage and sharp decline in fluid output of production wells in the polymer injection zone of the Henan oilfield, physical modeling has been used to study the blockage mechanism and blockage locations of the polymer-flooded reservoir based on oil reservoir characteristics and blockage knowledge. The results show that all the constant pressures in the low, moderate, and high permeability cores subjected to polymer injection and subsequent waterflooding were higher than the constant pressure during primary waterflooding; hence, polymer retention and blockage phenomena were obvious in the cores; in the high permeability core, the pore surface adsorbed more polymer molecules though pore throat radii were still much greater than the size of the polymer molecule, suggesting that polymer blockage is mainly caused by adsorption and retention. For the low permeability core, the specific surface area of the inlet end was much larger than that in the high permeability core, leading to more serious capture of polymer molecules at the small pores, indicating that blockage under polymer injection is mainly caused by capture and retention; for the lower permeability (91.81 mD) core, as compared with the case prior to polymer injection, the polymer-injected core had fewer large pores and throats, the mean pore throat radius decreased from 42.2 μm to 39.9 μm, and the mean throat-to-pore coordination number decreased from 3.36 to 3.19; thus, polymer capture and retention led to core blockage; the leftward shift of the curve corresponding to the porosity component, high porosity peak weakening after polymer injection, moderate and low porosity peaks appearing after polymer injection, and enhancement of lower porosity peaks indicate that, after polymer injection and subsequent waterflooding, polymer adsorption and capture led to blockage of some large pores; the highest pressure gradient, i.e., 6.3 MPa/m, was achieved at the P2-P3 segment; thus, the worst blockage occurred at the P2-P3 stage, or 1/8-1/4 of the sandpack length. In this paper, Nanbaxian oil and gas field, China, was taken as an example to investigate the interpretation method of gas saturation in a complex pore structure. The "four properties" relationship of the formation reservoir in the Nanbaxian oil and gas field was studied in depth according to the conventional logging data and core analysis data. The neural network algorithm was used to reconstruct the resistivity curve of the water layer to eliminate the influence of lithology, shale content, and pore structure on the resistivity. The difference between the reconstructed curve and the measured resistivity curve was used to identify the gas and water, and the ratio of the two was used to calculate the gas saturation, and good results were achieved. It was found that the sedimentary types of the Nanbaxian oil and gas field cause the reservoir to be thin, numerous, and dispersed; the lateral correlation is difficult. In addition, the structural features lead to the reservoir types being various in the vertical direction, which makes the identification of reservoir fluid more difficult. The results revealed that the rock compaction, poor physical properties, complex pore structure, high resistivity of surrounding rocks, and low formation water salinity make the water layer with high resistivity and difficult to identify gas and water.

1. Introduction

In most of the oilfields exploited by waterflooding for a long time in China, the reservoirs become increasingly heterogeneous, with water cuts increasing constantly [1–3]. Use of polymer flooding is able to improve effectively the water-to-oil mobility ratio and expand the macroscopic sweeping volume so as to enhance the oil recovery [4–6]. Polymer flooding technology has been applied on an increasingly larger scale in onshore oilfields in China, including Henan oilfield [7, 8]. With the increase in polymer injection time, the increased injection volume leads to prolonged polymer

Table 1: Data of the cores selected for the study.

Cored block	Core no.	Length (cm)	Diameter (cm)	Porosity	Permeability (mD)	Total pore volume (cm^3)
VII Upper	7-145-7	7.40	2.5	0.18	7.46	36.33
VII Upper	7-145-21	9.32	2.5	0.22	450.25	45.75
VII Upper	7-145-22	8.00	2.5	0.21	91.81	39.25
Shuanghe North	431-3	8.64	2.5	0.18	355.77	42.36
Shuanghe North	431-6	5.71	2.5	0.16	292.59	28.01

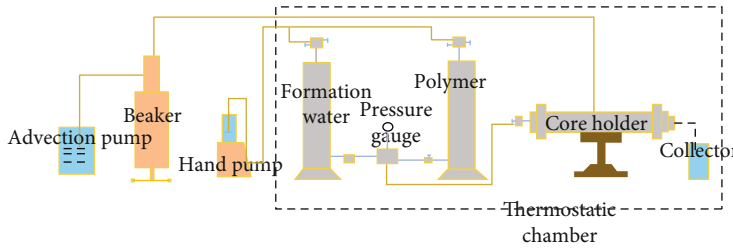

Figure 1: Flowchart of core displacement test.

buildup, resulting in commonplace blockage issue of oil bottoms and near-well zones [9–11]; hence, some polymer-injected wells experienced surging injection pressure, smaller injectivity index, failing to meet the requirements for injection proration, etc. [12, 13], having many detrimental effects on subsequent oilfield production.

In the past years, some knowledge about the causes of polymer-injected well blockage has been obtained under high attention of researchers worldwide [14–16]. In a mobility test of the Berea core, Dovan et al. [17] observed injection difficulty after prolonged flooding and attributed it to blockage due to intertwining of the retained polymer molecules. When evaluating the effectiveness of polymer flooding in Taber South oilfield, Shaw and Stright [18] found that "fish eyes" and other insoluble micelles arising from incomplete polymer maturation would cause blockage to some extent in the near-well zone, seriously impairing the effectiveness of polymer flooding. Likewise, after analysis of field flowback fluid, Zhen et al. [19] believed that the polymer solution containing "fish eyes" is a major contaminant of the polymer-injected well. Tang et al. [20] studied adsorption behavior of the stationary-state solution of partially hydrolyzed polyacrylamide onto polymer-flooded rock in Daqing oilfield. The results show that clay minerals play a leading role in polymer adsorption; adsorption capacities of a polymer on clay minerals were 4–10 times that of the rock matrix, impeding fluid flow so as to block the formation. Lu and Gao [21] found in a polymer flooding study that there is compatibility relationship between dimensions of polymer molecular coils and rock core; poor compatibility is prone to formation of plugs, hampering subsequent polymer injection. Based on a conceptual model of numerical simulation featuring 1-injection-1-production, Qu et al. [22] studied the effect of polymer plugging position on production performance of the oil reservoir by means of equivalent characterization with a well index of the well point and connectivity between wells and established a diagnostic plot of polymer plugging positions. Zhu [23] simulated numerically the conditions of polymer-flooded reservoir in Beierxi district and found that, in development blocks with an injection-production well spacing of 250 m, polymer solution was mainly retained within the first 40 m, and the most significant retention occurred within the first 20 m; based on injection-production performance of scaled-up well group SZ36-1-A07, Zeng [24] employed an injection-production performance data fitting method to infer that the blockage of a polymer-injected well mainly occurs in the near-well zone and the greatest pressure gradient change occurred within a radius of 60 m from an injection well in oilfield blocks such as SZ36-1-A07 with a well spacing of 350 m and thereby concluded that polymer retention was mainly concentrated within a radius of 60 m from a polymer-injected well and the most significant retention occurred within the first 25 m. All the above conclusions on plugging positions were inferred by numerical simulation and injection-production performance data fitting. By using long sandpacks, the authors studied blockage positions of the polymer-injected reservoir and concluded that the worst blockage occurred at 1/8–1/4 of sandpack length. Furthermore, based on geological characteristics and fluid properties of polymer-flooded reservoirs in the Henan oilfield, research of the reservoir blockage mechanism and other aspects was carried out by means of scanning electron microscopy (SEM), CT, and nuclear magnetic resonance spectrometry (NMR), and systematic knowledge was obtained, which is of significant guidance on subsequent field application and performance adjustment and offers theoretical support for effective application of polymer flooding technology in the Henan oilfield.

2. Experimental

2.1. Apparatus and Materials. The following are the apparatus and materials used: two-dimensional plane modeling evaluation test apparatus, 2PB00C advection pump,

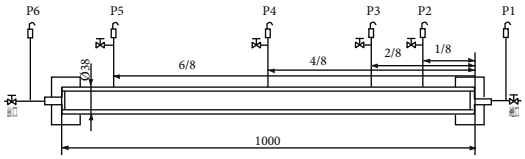

Figure 2: Experimental model of multipoint pressure measurement for long core sandpack.

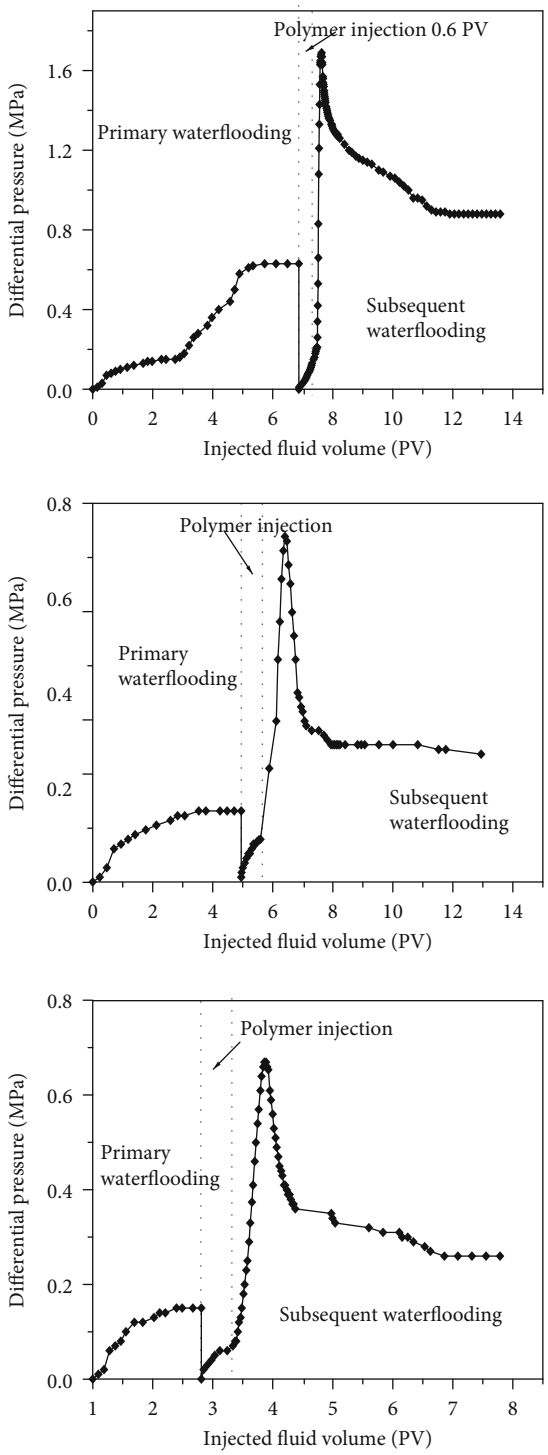

Figure 3: Analysis of core pressure curves.

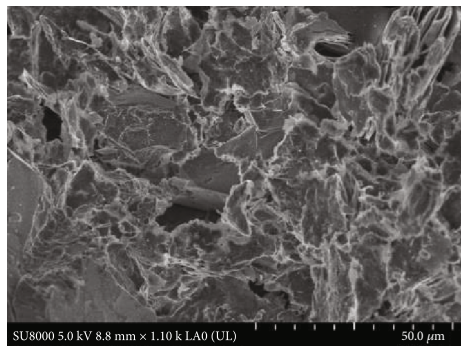

Figure 4: Microstructural image of the core at its inlet end (magnification: 1100x).

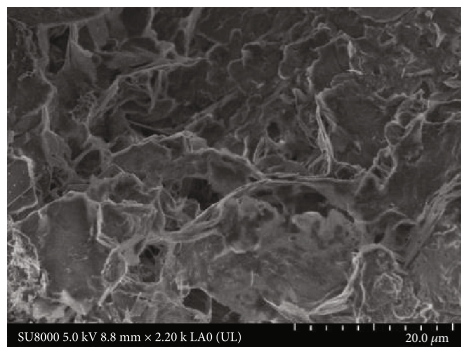

Figure 5: Microstructural image of the core at its inlet end (magnification: 2200x).

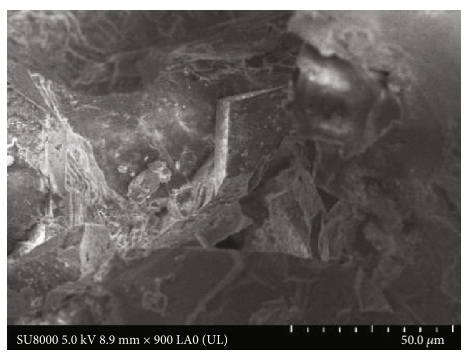

Figure 6: Microstructural image of the core at its outlet end.

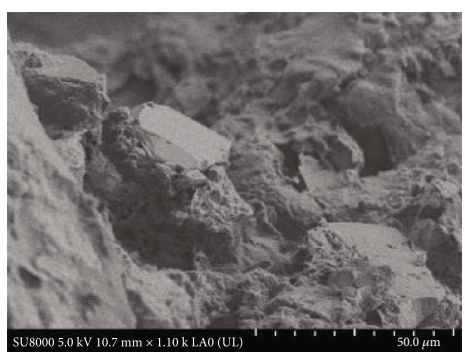

Figure 7: Microstructural image of the core at 0–1/8 of the full sandpack length (magnification: 2000x).

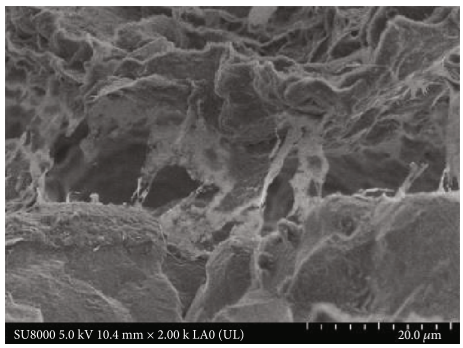

Figure 8: Microstructural image of the core at 0–1/8 of the full sandpack length (magnification: 4500x).

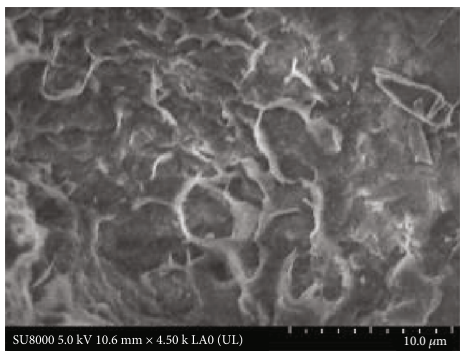

Figure 9: Microstructural image of the clean core.

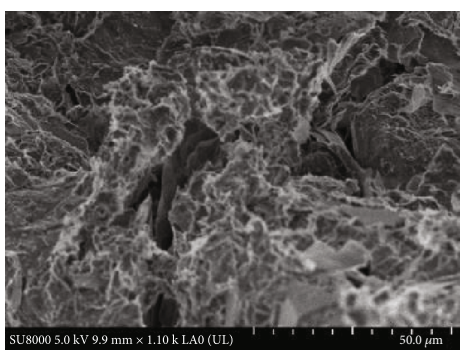

Figure 10: Microstructural image of the core at 1/8–1/4 of the full sandpack length (magnification: 1100x).

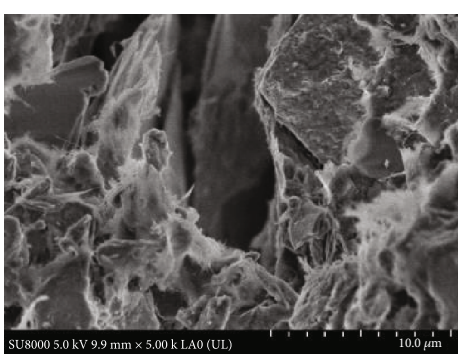

Figure 11: Microstructural image of the core at 1/8–1/4 of the full sandpack length (magnification: 5000x).

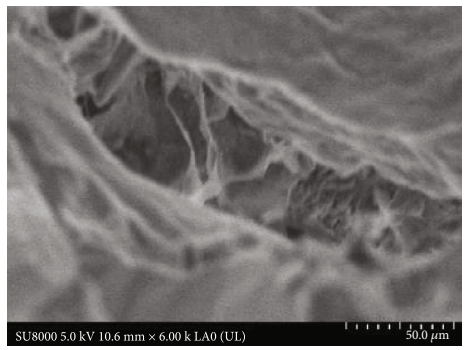

Figure 12: Microstructural image of the core at 1/8–1/4 of the full sandpack length (magnification: 6000x).

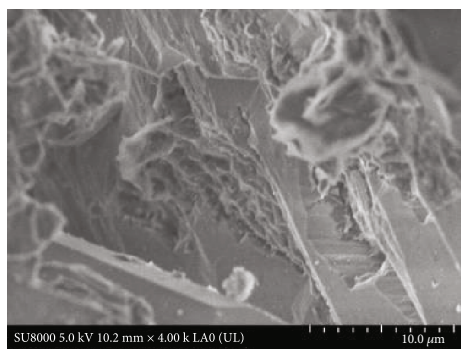

Figure 13: Microstructural image of the core at 1/4–1/2 of the full sandpack length.

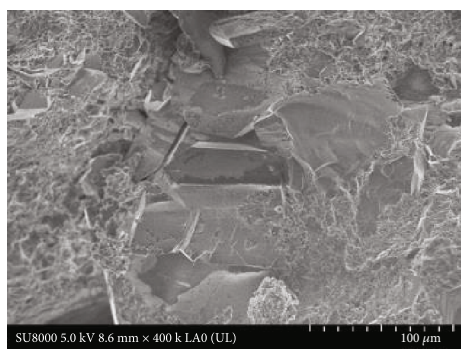

Figure 14: Microstructural image of the core at 1/2–3/4 of the full sandpack length.

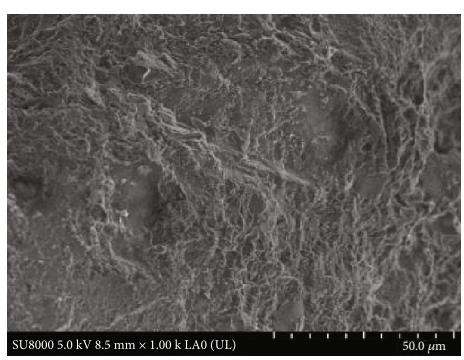

Figure 15: Microstructural image of the core at tail end.

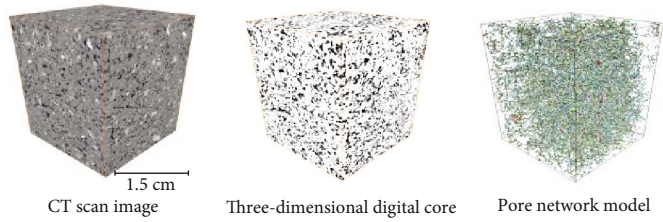

Figure 16: CT scan image and modeling of some of the core regions prior to polymer injection.

micrometer-nanometer double-ray tube CT scan system for rock cores, SU8010 field-emission SEM, NMR instrument suite, pressurized vacuum saturation apparatus, high-speed refrigerated centrifuge, NMR tight core analyzer, sandpack, feldspar powder, calcite powder, quartz sand, and polymer (molecular weight: 28.63 million).

The oil sample is Shuangguan Well No. 1, the northern block of the Shuanghe oilfield; the water sample is the northern block of the Shuanghe oilfield; formation water is $NaHCO_3$ type, $Na^+ + K^+$ 2725 mg/L, Cl^- 3120 mg/L, SO_4^{2-} 1100 mg/L, HCO_3^- 1100 mg/L, CO_3^{2-} 360 mg/L, and total salinity 8405 mg/L; the core data of the cores for this study are shown in Table 1.

2.2. Methodology

2.2.1. Columnar Core Displacement Test

(1) Test flowchart

(2) Test procedure (see Figure 1)

(i) Saturate the core with formation water at a flow rate of 0.5 mL/min and test it to obtain core data

(ii) Inject polymer solution into the core until 0.6 PV

(iii) Run subsequent waterflooding at a flow rate of 0.5 mL/min and collect repeatedly the produced fluid at the production end with a 5 mL graduated cylinder until polymer concentration of the produced fluid equilibrates and approximates to zero, then stop injection

(iv) End the test

2.2.2. SEM Scan. Each polymer-injected core was cross-sectioned at different locations; the core sections were then lyophilized, followed by SEM scan of their surface topography using SU9000 Hitachi SEM.

2.2.3. CT Scan. Fracture development in the undamaged core was understood via a micrometer-nanometer double-ray tube CT scan system for rock cores, which differs from the general method for studying the reservoir bed in that processes such as oil washing are not required and it can be carried out while the core remains in its initial state. This CT scan system enables a straightforward description of rock properties such as porosity distribution, fractures, pores, and rock damages, as well as quantitation of rock attributes such as porosity, pore-to-throat size ratio, shape factor, connectivity, coordination number, absolute permeability, relative permeability, and capillary pressure. From the above qualitative description and quantitative calculation of CT data, the polymer plugging mechanism for polymer-injected wells was further determined.

2.2.4. NMR Analysis. Out of one-dimensional NMR T2 spectral techniques, the low-field NMR core analysis technique has been successfully applied in calculation of petrophysical parameters such as porosity, irreducible water saturation, and movable fluid saturation, estimation of permeability, and evaluation of pore structure, playing an important role in oil exploration and exploitation. In this paper, core NMR measures and acquires the core echo train attenuation curve based on CPMG pulse sequence, followed by inversion to obtain such parameters as T2 distribution, T2 cutoff value, geometric T2 mean, and arithmetic T2 mean, so as to calculate core information including total porosity, permeability, movable fluid saturation, and irreducible fluid saturation, which can be applied to basic evaluation of reservoir parameters such as physical properties so as to determine the blockage mechanism for polymer-injected wells.

2.2.5. Multipoint Pressure Measuring Test Based on Long Core Sandpack. A long sandpack (dimensions: $L = 1000$ mm, $\Phi = 36$ mm) was used to study blockage locations of the polymer-injected reservoir. Pressure measuring points were set at 1/8, 1/4, 1/2, and 3/4 of full sandpack length from the inlet end, respectively, denoted as P2 through P5, respectively, and pressure measuring points P1 and P6 were set at the inlet end and outlet end, respectively, totaling six pressure measuring points (see Figure 2). Variability patterns of pressures at six pressure measuring points during polymer injection were explored; pressure gradients between neighboring pressure measuring points were calculated and compared, so as to determine plugging positions of polymer solution. The test procedure is the following: (1) saturate the sandpack with formation water at a rate of 5 mL/min and acquire sandpack data; (2) saturate the sandpack with crude oil at a rate of 1 mL/min; (3) run primary waterflooding at a rate of 1 mL/min and record the recovery efficiency and inject the polymer when water cut reaches 98%; (4) inject polymer solution into the sandpack until 0.6 PV; and (5) run subsequent waterflooding at a rate of 3 mL/min and collect the produced fluid at the outlet end while recording the pressure changes during subsequent waterflooding.

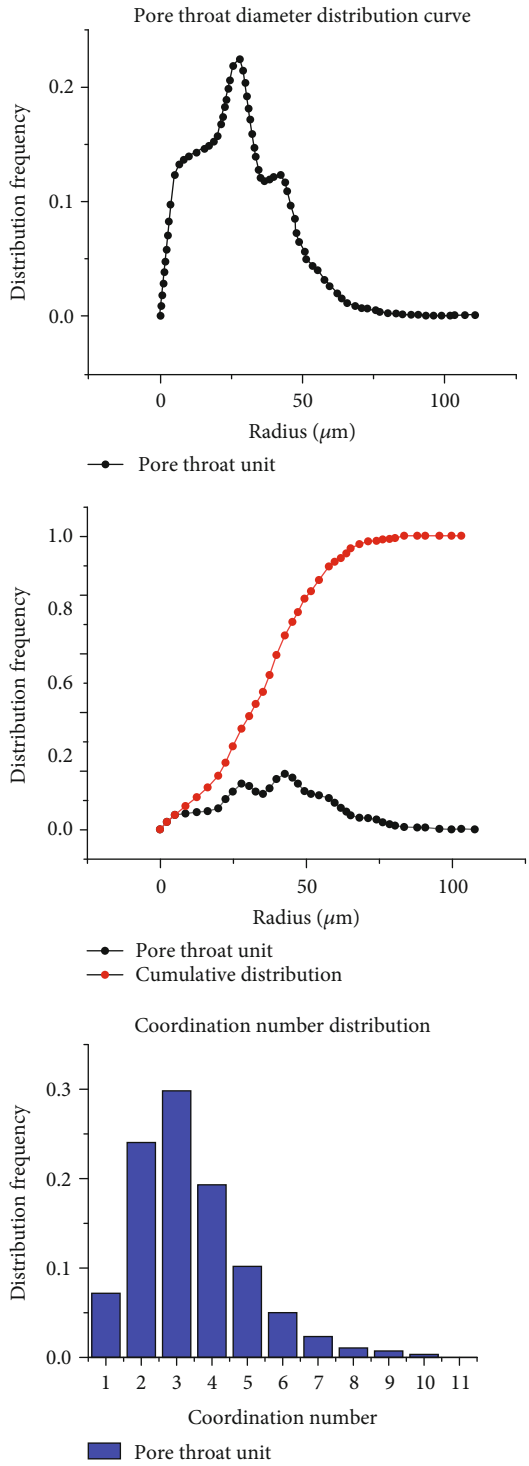

Figure 17: Curves of quantified CT data of the core prior to polymer injection.

3. Results and Discussion

3.1. Core Displacement Test. As can be seen from the pressure curves of the low permeability core, the moderate permeability core, and the high permeability core in Figure 3, constant pressures during subsequent waterflooding were all higher than those during primary waterflooding. Thus, polymer retention in the core was obvious, resulting in reservoir blockage that affected subsequent waterflooding.

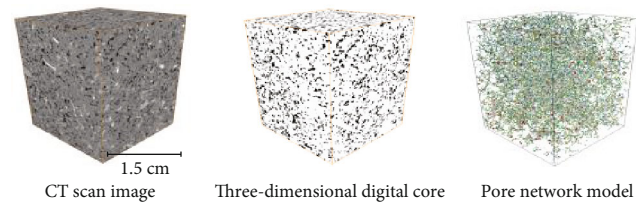

Figure 18: CT scan image and modeling of some of the core regions after polymer injection.

3.2. SEM Scan. In order to further determine the blockage mechanism during polymer injection, core ends were sectioned prior to and after polymer injection, respectively, naturally dried, and coated with gold by sputtering, followed by SEM examination of their microstructures. The following figures show SEM results of core samples from Shuanghe North Block differing in permeability.

3.2.1. Rock Core of 7.46 mD in Permeability. Micrographs of the inlet end of the core in Figures 4 and 5 show that, from the microscopic perspective, the specific surface area of the low permeability core was much larger than that of the high permeability core, with many more cracks, throats, and angles than in the case of the high permeability core; hence, capture of polymer molecules at small pores was serious, leading to increased retention due to polymer capture and thus serious polymer plugging. The micrograph of the outlet end of the core in Figure 6 shows that fewer polymer molecules were adsorbed by the core surface at the tail end and captured by small pores there; thus, core blockage was milder.

3.2.2. Rock Core of 355 mD in Permeability. Figures 7 and 8 show that, compared with the microstructural image of the clean core in Figure 9, on the core at 0–1/8 of the full sandpack length, the pore surface adsorbed more polymer molecules, though pore throat radii were still much larger than the polymer molecular size, suggesting that blockage in polymer injection is mainly caused by adsorption and retention.

Figures 10–12 show that bare particles of the rock had large surface areas; these particle surfaces and pore surfaces adsorbed a great number of polymer molecules after polymer injection and formed an adherent layer, indicating that blockage in polymer injection is mainly caused by adsorption and retention.

Figure 13 shows that, compared with blockage in the core at 1/8–1/4 and 0–1/8 of the full sandpack length, the core surface at 1/4–1/2 of the full sandpack length adsorbed fewer polymer molecules, resulting in milder core blockage; Figures 14 and 15 show that the core surfaces at 1/2–3/4 of the full sandpack length and the tail end adsorbed even fewer polymer molecules, resulting in minimum core blockage.

3.3. CT Scan. Capillaries of different radii were used in the model; these capillaries were randomly distributed in the network. This model was employed to study network features including capillary pressure and relative permeability; it is

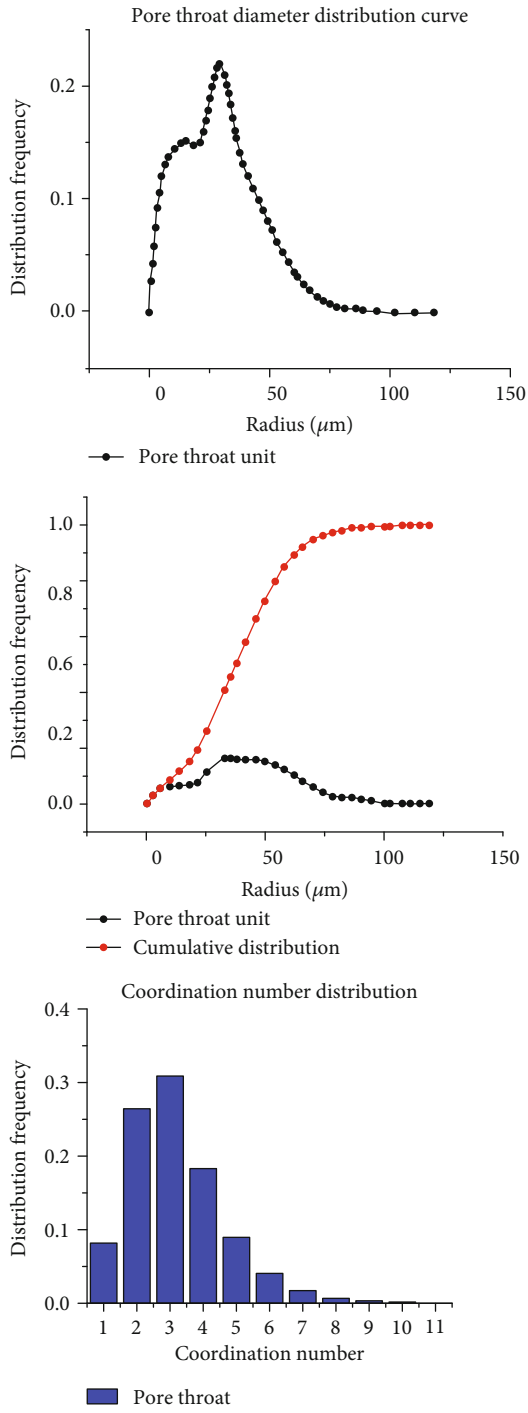

Figure 19: Curves of quantified CT data of the core after polymer injection.

capable of predicting macroscopic properties of rock very well, including coordination number, i.e., number of throats connected by each pore in the core.

3.3.1. VII Upper Shuang K7-145-22 Core prior to Polymer Injection. Figures 16 and 17 show that, prior to polymer injection, the core contained a great quantity of pores and throats, offering conditions for effective seepage of the polymer, oil, and water.

3.3.2. VII Upper Shuang K7-145-22 Core after Polymer Injection. Figures 18 and 19 show that, in the low permeability (91.81 mD) core, there were fewer large pores and throats after polymer injection as compared with the case prior to polymer injection, mean pore throat radius decreased from 42.2 μm to 39.9 μm, and mean throat-to-pore coordination number fell from 3.36 to 3.19; thus, polymer capture and retention caused core blockage.

3.4. NMR Analysis. Nuclear magnetic relaxation will give rise to induction current, i.e., NMR signal (content of hydrogen protons), and T2 spectrum illustrates the hydrogen proton content-nuclear magnetic relaxation time curve. NMR signal relaxation time is closely related to ambience of hydrogen nuclei, and T2 is capable of acquiring more accurate results at a faster rate on-site; thus, T2 signal alone is acquired in current logging practice. Signal processing technique is able to convert the acquired T2 information into T2 distribution.

Figure 20(a) shows that, for the high permeability core, the whole polymer injection curve shifts to the left relative to the curve corresponding to water saturation, and the number of apparent small pores increased, indicating that polymer adsorption led to blockage of large pores after completion of polymer injection and subsequent waterflooding. Figure 20(b) shows that, for the moderate-to-high permeability core, the peak corresponding to high porosity attenuated while the peak corresponding to low porosity was enhanced in the polymer injection curve. Figure 20(c) shows that, for the low permeability core, the peak corresponding to higher porosity attenuated while the peaks corresponding to lower porosity and moderate porosity were enhanced in the polymer injection curve, indicating that mechanical capture of the polymer led to pore blockage after completion of polymer injection and subsequent waterflooding.

3.5. Sandpack Test. Based on the study on the blockage mechanism for the polymer-flooded reservoir, the reservoir blockage locations were further investigated by measuring pressure gradients between pressure measuring points with a sandpack, and the test results are shown in Figure 21.

The pressure gradient-injection volume curves in Figure 21 show that the pressure gradient between pressure measuring points P2 and P3 was the maximum, i.e., 6.3 MPa/m, indicating that the blockage occurred between P2 and P3; thus, serious blockage occurred at the P2-P3 segment, i.e., 1/8–1/4 of full sandpack length.

In order to further identify the reservoir blockage locations, the characteristics of pressure propagation between injection and production wells with a sandpack and the test results are tabulated as follows.

The pressure propagation data in Table 2 show that, given injection volumes of 10 PV–12 PV, the pressure at P1 increased from 1.018 MP to 2.152 MP, the pressure at P2 increased from 0.440 MP to 1.729 MP, and the pressure at P3 increased from 0.125 MP to 1.070 MP; the rise in pressure at P2 was the most significant, and the increment was 1.289 MP, so serious blockage occurred within P2-P3, i.e., at 1/8–1/4 of full sandpack length.

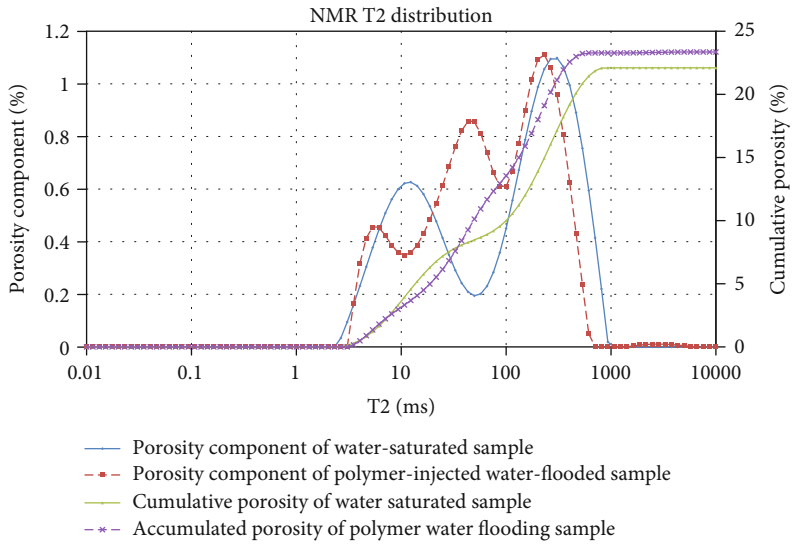

(a) NMR T2 distribution spectra before and after polymer injection into Shuang K7-145-21 core from Shuanghe North Block

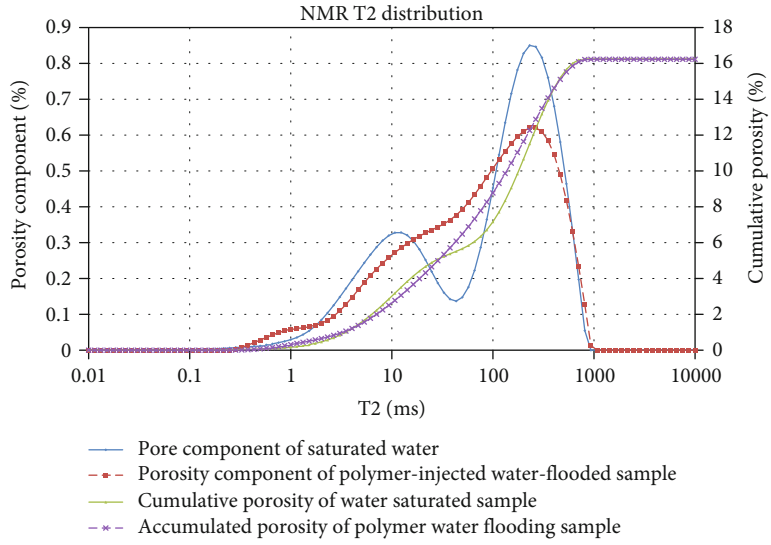

(b) NMR T2 distribution spectra before and after polymer injection into Shuang K431-6 core from Shuanghe North Block

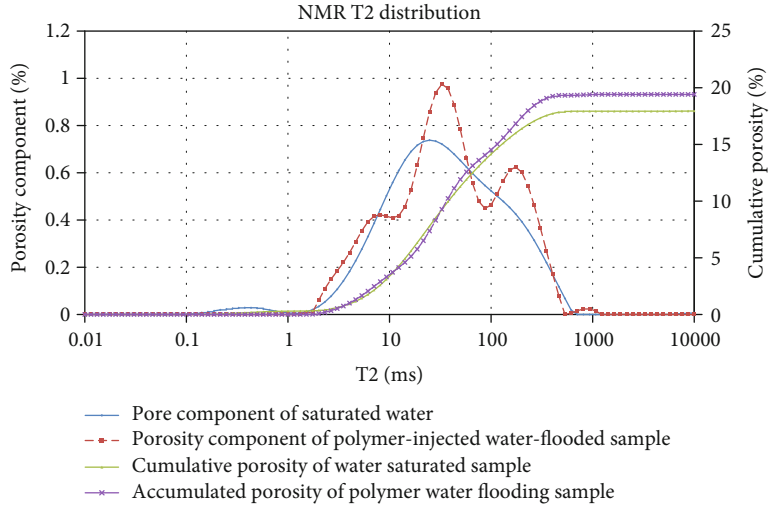

(c) NMR T2 distribution spectra before and after polymer injection into Shuang K7-145-7 core from Shuanghe North Block

Figure 20: NMR T2 distribution spectra.

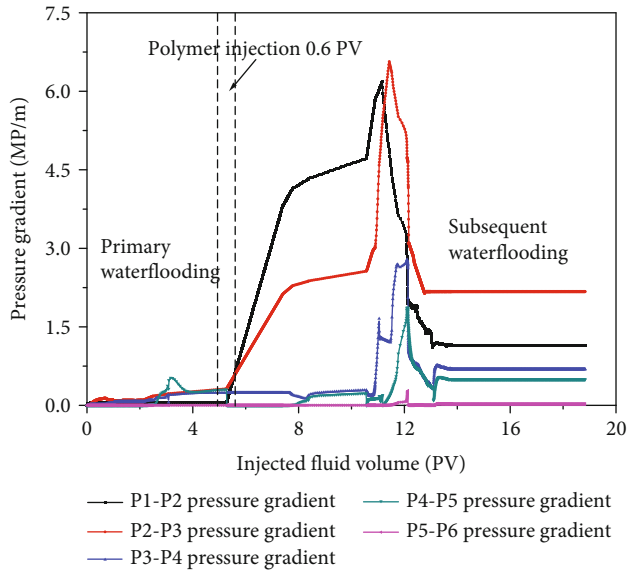

Figure 21: Pressure gradient versus injection volume.

Table 2: Pressure propagation data at pressure measuring points on the sandpack.

Number of PVs injected	Pressure measuring point P1	Pressure measuring point P2	Pressure measuring point P3	Pressure measuring point P4	Pressure measuring point P5	Pressure measuring point P6
1.00	0.031	0.025	0.013	0.000	0.000	0.000
1.50	0.037	0.030	0.018	0.000	0.000	0.000
2.00	0.037	0.030	0.018	0.000	0.000	0.000
2.50	0.058	0.052	0.029	0.005	0.000	0.000
5.28	0.181	0.175	0.135	0.076	0.000	0.000
5.88	0.304	0.164	0.059	0.000	0.000	0.000
7.00	0.669	0.282	0.059	0.000	0.000	0.000
9.00	0.970	0.414	0.110	0.048	0.000	0.000
10.00	1.018	0.440	0.125	0.055	0.000	0.000
12.00	2.152	1.729	1.070	0.396	0.018	0.000
15.00	0.716	0.573	0.301	0.129	0.006	0.000
18.83	0.716	0.573	0.301	0.129	0.006	0.000

4. Summary

(1) As known from polymer injection testing of the low permeability, moderate permeability, and high permeability natural cores, all constant pressures during subsequent waterflooding were higher than those during primary water flooding; thus, polymer retention phenomena in the cores were obvious, leading to blockages to some extent

(2) Based on SEM scan, in the high permeability core, the pore surface adsorbed more polymer molecules though pore throat radii were still much greater than the size of the polymer molecule, indicating that polymer blockage is mainly caused by adsorption and retention. For the low permeability core, the specific surface area of the inlet end was much larger than that for the high permeability core, and there were many more cracks, throats, and angles than the case of the high permeability core, resulting in more serious capture of polymer molecules in small pores, indicating that the blockage under polymer injection is mainly caused by capture and retention

(3) Based on CT scan, for the lower permeability (91.81 mD) core, there were fewer large pores and throats in the core after polymer injection as compared with the case prior to polymer injection, mean pore throat radius decreased from 42.2 μm to 39.9 μm, and mean throat-to-pore coordination number fell from 3.36 to 3.19; thus, polymer capture and retention resulted in core blockage

(4) Based on NMR T2 spectra, the curves corresponding to porosity component shift to the left, and after polymer injection, high porosity peaks attenuated, low-to-moderate porosity peaks appeared, and the peaks corresponding to lower porosity became enhanced, indicating that polymer adsorption and capture led to blockage of some large pores after completion of polymer injection and subsequent waterflooding

(5) From the perspective of physical modeling, the maximum pressure gradient was achieved within the P2-P3 segment, i.e., 6.3 MP/m; thus, the worst blockage occurred within the P2-P3 segment, i.e., at 1/8–1/4 of full sandpack length. The pressure propagation data in Table 2 show that, given injection volumes of 10 PV–12 PV, the pressure at P1 increases from 1.018 MP to 2.152 MP, the pressure at P2 increased from 0.440 MP to 1.729 MP, and the pressure at P3 increased from 0.125 MP to 1.070 MP, though the pressure rise at P2 was the most significant, and the increment was 1.289 MP; therefore, serious blockage occurred within P2-P3, i.e., at 1/8–1/4 of full sandpack length

Data Availability

The [data type] data used to support the findings of this study are included within the supplementary information file(s).

Conflicts of Interest

Yu Li and coauthors have no conflict of interest.

Acknowledgments

This study has been supported by the Sinopec Key Technology R&D Program "Study on Composite Blockage Removal Technology for Polymer-Flooded Blocks" (P20070-6).

References

[1] Y. L. Li, R. Niu, R. Z. You, X. J. Yin, L. X. Cong, and Z. Li, "Study of reversal characteristics of polymer flooding profile for multilayer heterogeneous reservoirs," *Fault-Block Oil & Gas Field*, vol. 27, no. 6, pp. 794–798, 2020.

[2] B. Xu, "Experimental study of distribution characteristics of remaining oil with gel profile control in longitudinal heterogeneous reservoirs," *Petroleum Geology and Recovery Efficiency*, vol. 27, no. 6, pp. 71–80, 2020.

[3] S. Zhao, W. F. Pu, K. X. Li, and Y. Yang, "Study on heterogeneous profile control capability of polymer microspheres," *Reservoir Evaluation and Development*, vol. 9, no. 4, pp. 51–56, 2019.

[4] D. Liu, Y. P. Li, F. Y. Zhang, C. Q. Zhang, and Y. K. Luo, "Study on factors that influence the use of weak gels to enhance recovery efficiency in offshore heavy-oil oilfields," *Special Oil & Gas Reservoirs*, vol. 20, no. 2, pp. 72–74, 2013.

[5] W. Y. Zhu, Y. A. Tian, W. D. Wang et al., "Microscopic flooding mechanism of endogenous emulsifying microorganisms in an oil reservoir against remaining oil," *Journal of Central South University (Natural Science Edition)*, vol. 47, no. 9, pp. 3280–3288, 2016.

[6] W. Y. An, "Study of interlayer interfering factors of a multilayer heterogeneous oil reservoir at the ultra-high water cut stage," *Journal of Northeast Petroleum University*, vol. 36, no. 5, pp. 76–82, 2012.

[7] M. L. Fu, J. C. Zhou, F. Xiong, C. Ye, R. H. Wang et al., "Study on blockage mechanism for crosslinked polymer-flooded reservoirs in the Henan oilfield," *Oilfield Chemistry*, vol. 27, no. 2, pp. 188–191, 2010.

[8] M. L. Fu and F. Xiong, "Study on blockage mechanism for polymer-flooded reservoirs in the Henan oilfield," *Drilling and Production Technology*, vol. 32, no. 4, pp. 77–79, 2009.

[9] J. Zou, L. Chen, C. L. Liu, S. Gao, and L. P. Zhang, "Blockage removal mechanism of β-cyclodextrin for amphiphilic polymer-like plugs in oilfields," *Oilfield Chemistry*, vol. 36, no. 3, pp. 440–443, 2019.

[10] S. Gao, Y. G. Liu, X. T. Lan, Y. Y. Fu, and C. L. Liu, "Analysis of plug components in polymer-injected wells in the Bohai oilfield and their interaction mechanism," *Oilfield Chemistry*, vol. 37, no. 2, pp. 340–343, 2020.

[11] D. Y. Lu, X. H. Meng, W. Wu, and J. Y. Zhou, "Study on blockage mechanism for polymer-injected wells in the Bohai oilfield and design of composite blockage removal technology," *China Offshore Oil and Gas*, vol. 28, no. 5, pp. 98–103, 2016.

[12] Z. H. Chen, W. H. Hou, and W. J. Liu, "Use of injectivity index curve to study the changes of oil reservoir properties after polymer flooding," *Petroleum Geology & Oilfield Development in Daqing*, vol. 22, no. 1, pp. 47–49, 2003.

[13] J. F. Xu, J. Q. Zhang, G. R. An, W. S. Zhou, and J. Shen, "Adjustment potential of injection-production system for offshore oilfields developed by water injection in China," *Petroleum Geology & Oilfield Development in Daqing*, vol. 35, no. 6, pp. 53–56, 2016.

[14] M. Y. Zeng, P. F. Zhao, K. Xu, J. Du, and L. Q. Zhao, "Laboratory study of addressing the blockage of polymer-injected wells with steady-state ClO_2 and acid solution together," *Drilling and Production Technology*, vol. 36, no. 1, pp. 98–101, 2013.

[15] X. L. Meng, L. Q. Zhao, K. Xu, and J. Q. Li, "Causes of polymer-injected well blockage and the blockage removal technology," *Oil Drilling and Production Technology*, vol. 33, no. 3, pp. 70–73, 2011.

[16] H. X. Chen, X. T. Lan, M. Pang, Y. Y. Fu, H. M. Tang et al., "Study on genesis of the plugs in wells benefiting from polymer injection in the Bohai oilfield," *Journal of Guangdong University of Petrochemical Technology*, vol. 30, no. 1, pp. 1–5, 2020.

[17] H. T. Dovan and R. D. D. Hutchins, *Dos cuadras offshore polymer flood*, Paper presented at the SPE California Regional Meeting, Ventura, California, 1990.

[18] R. A. Shaw and D. H. Stright Jr., "Performance of the Taber South polymer flood," *Journal of Canadian Petroleum Technology*, vol. 16, 1977.

[19] J. D. Zhen, Y. Z. Zhang, H. Ren, and Y. Liu, "Study on blockage mechanism and blockage removing agents for polymer-injected wells," *Petroleum Exploration and Development*, vol. 31, no. 6, pp. 109–111, 2004.

[20] H. M. Tang, Y. F. Meng, X. Yang, and Z. Chen, "Study on loss of polyacrylamide due to minerals in a reservoir," *Oilfield Chemistry*, vol. 18, no. 4, pp. 342–346, 2001.

[21] X. G. Lu and Z. H. Gao, "Compatibility between polymer molecular weight and core permeability—ratio of pore throat

radius to radius of gyration of polymer molecular coil," *Oilfield Chemistry*, vol. 13, no. 1, pp. 72–75, 1996.

[22] Z. Z. Qu, Y. L. Li, L. L. Wang, F. J. Zhou, and X. R. Wang, "Quantitative characterization of blockage locations in offshore polymer-flooded oil reservoirs," *Fault-Block Oil & Gas Field*, vol. 26, no. 3, pp. 360–363, 2019.

[23] G. B. Zhu, *Study on Blockage Removal and Injection Stimulation Technology for Polymer-Injected Wells*, Daqing Petroleum Institute, Daqing, 2007.

[24] M. Y. Zeng, *Study on High-Performance Blockage Removal Technology for Polymer-Injected Wells in an Offshore Oilfield*, Southwest Petroleum University, Chengdu, 2013.